Supporting Information for "A minimal computational model for three dimensional cell migration"

FULL MODEL

Our three-dimensional model for the cell boundary and cell motion is extended from earlier studies [1–3] in two dimensions. Briefly, we model the cell boundary as an interface with tension and bending, driven by an activator A. Cell motion obeys the overdamped force balance equation $\boldsymbol{F}_{act} + \boldsymbol{F}_{mem} + \boldsymbol{F}_{sub} + \boldsymbol{F}_{geo} + \boldsymbol{F}_{fric} = 0$ where $\boldsymbol{F}_{act}$ is the active force proportional to the activator concentration, $\boldsymbol{F}_{mem}$ describes the membrane tension, $\boldsymbol{F}_{sub}$ is the cell-substrate forces like adhesion, and $\boldsymbol{F}_{fric}$. Furthermore, and based on our experiments that show that the total cell membrane and volume does not change during migration (Fig. S1), $\boldsymbol{F}_{geo}$ represents surface and volume conservation. Note that we do not explicitly model the traction force patterns that have been obtain in experiments [4, 5]. This could be accomplished by including actin flow, as carried out in earlier work [2], or in models which greatly simplifies morphologies [6].

The active force from the activator is governed by $\boldsymbol{F}_{act} = \eta(z)M(A)\hat{\boldsymbol{n}}$, where $\hat{\boldsymbol{n}} = -\nabla\phi/|\nabla\phi|$ is the outward-pointing normal direction of the membrane, and $M(A) = A/(A + A_0)$ where A_0 represents a threshold value for activation of A. One key assumption in our model is that the active protrusive force depends on the distance z from the substrate. In simulations, we put the substrate at $z = 0$, and the protrusive force is

$$\eta(z) = \frac{\eta_0}{4}[3 - \tanh(\frac{z-h}{h_0})], \tag{S1}$$

which represents a protrusive force that smoothly changes from approximately η_0, close to the substrate, to $\eta_0/2$ far away from the substrate, with a maximal gradient at $z = h$. The parameter h_0 represents the width of the region where the protrusive force changes from η_0 to $\eta_0/2$. We have verified that other functional forms in which the protrusive strength varies smoothly between these two values give qualitative similar results.

The membrane tension is computed using the functional derivative [3] $\boldsymbol{F}_{mem} = \frac{\delta H(\phi)}{\delta\phi}\nabla\phi/\delta_\epsilon$, with $\delta_\epsilon = \epsilon|\nabla\phi|^2$ and

$$H(\phi) = \gamma\int(\frac{\epsilon}{2}|\nabla\phi|^2 + \frac{G(\phi)}{\epsilon})d^3\boldsymbol{r}. \tag{S2}$$

Here, $G(\phi)$ is a double well potential with minima at $\phi = 1$ and $\phi = 0$: $G(\phi) = 18\phi^2(1-\phi)^2$. Note that the cell membrane can be tracked by the phase field:

$$\psi = 2\frac{G(\phi)}{\epsilon}. \tag{S3}$$

The location of the substrate is determined by χ, with $\chi = 1$ indicating the substrate into which the cell cannot penetrate, and $\chi = 0$ indicating the region accessible to the cell:

$$\chi(z) = \frac{1}{2}[1 + \tanh(\frac{3z}{\epsilon})], \tag{S4}$$

The interaction between the cell membrane and substrate is represented by $\boldsymbol{F}_{sub} = \frac{\delta H(\phi,\chi)}{\delta\phi}$ with

$$H(\phi,\chi) = \int d^3\boldsymbol{r}\phi^2(\phi-2)^2[-2f_{adh}\frac{G(\chi)}{\epsilon} + f_{rep}\chi(z+\epsilon)], \tag{S5}$$

similar to[7]. Here, f_{adh} is the adhesive strength between the cell membrane and the substrate and f_{rep} is a parameter that measures the penalty of overlap between cell and substrate [3]. Note that we can use a similar strategy to incorporate substrates with more complex geometries, for example in the form of capillaries or fibrous networks. Defining a field as in Eq. S4 will allow us to identifiy the location of this substrate and can, for example, be used to define a protrusive strength that depends on the distance from the substrate (see Eq. S1).

We implement surface and volume conservation as $\boldsymbol{F}_{geo} = [B_S(\int\psi d^3\boldsymbol{r} - S_0) + B_V(\int\phi d^3\boldsymbol{r} - V_0)]\hat{\boldsymbol{n}}$ where B_S, B_V represent the strength of the surface and volume conservation and S_0, V_0 is the prescribed surface size and volume, respectively. The friction is $\boldsymbol{F}_{fric} = \xi\boldsymbol{v}$ so that $\boldsymbol{v}$ is obtained from the force balance equation: $\boldsymbol{v} = (\boldsymbol{F}_{act} + \boldsymbol{F}_{mem} + \boldsymbol{F}_{sub} + \boldsymbol{F}_{geo})/\xi$ where all forces are defined per unit area. The motion of the phase field ϕ is then determined by the

advective equation $\partial\phi/\partial t = -\boldsymbol{v}\cdot\nabla\phi$. Finally, coupling the phase field equations to the reaction-diffusion equations presented in the main text, we arrive at the full equations:

$$\frac{\partial(\psi A)}{\partial t} = D_A\nabla\cdot(\psi\nabla A) + \psi[(\frac{k_a A^2}{K_a^2+A^2}+b)A_{cyt} - (d_1+d_2R)A + \zeta_1(t)], \tag{S6}$$

$$\frac{\partial(\psi R)}{\partial t} = D_R\nabla\cdot(\psi\nabla R) + \psi[\frac{c_2A - c_1R}{\tau} + \zeta_2(t)], \tag{S7}$$

$$\xi\frac{\partial\phi}{\partial t} = \eta(z)M(A)|\nabla\phi| + \gamma(\nabla^2\phi - \frac{G'(\phi)}{\epsilon^2}) + (\boldsymbol{F}_{sub}+\boldsymbol{F}_{geo})\cdot\nabla\phi. \tag{S8}$$

Notice that the reaction-diffusion process only happens at the cell membrane ψ and $A_{cyt} = (N_{tot} - \alpha\int A\psi d^3\boldsymbol{r})/V_0 = A_{tot} - \alpha\int A\psi d^3\boldsymbol{r}/V_0$. The parameters of the mechanic module, including tension and adhesion, are taken from [3, 7]. The parameters of the biochemical module (k_a, K_a, etc.) are estimated from experiments [8, 9] and follow our previous work [10]. Cell morphology parameters such as surface size and volume are estimated from experimental measurements. We have verified that changing the parameters of the biochemical module or the tension and adhesion parameters by $\pm$ 10% did not alter the qualitative results.

NUMERICAL DETAILS

The parameters used for numerical simulations are listed in Table S1. Equations are evolved in a region of size $L_x\times L_y\times L_z = 20\times20\times20\mu$m with discrete grids of $n\times m\times l = 128\times128\times128$ and periodic boundary conditions. Eq.S8 is discretized using the forward Euler method with $\partial_t\phi = (\phi^{(n+1)}-\phi^{(n)})/\Delta t$. Derivatives are calculated using finite difference formulas: $\partial_x\phi = (\phi_{i+1,j}-\phi_{i-1,j})/(2\Delta x)$ and $\partial_x^2\phi = (\phi_{i+1,j}+\phi_{i-1,j}-2\phi_{i,j})/\Delta x^2$, with similar equations for the derivatives in the y,z-direction. $\phi^{(n+1)}$ is determined by a semi-implicit form

$$\phi^{(n+1)} - \frac{\Delta t\gamma}{\xi}\nabla^2\phi^{(n+1)} = \frac{\Delta t}{\xi}[\eta(z)M(A)|\nabla\phi^{(n)}| - \gamma\frac{G'(\phi^{(n)})}{\epsilon^2} + (\boldsymbol{F}_{sub}+\boldsymbol{F}_{geo})\cdot\nabla\phi^{(n)}]$$

and solved by Fourier transform

$$\phi_{\boldsymbol{k}}^{(n+1)} = \frac{\phi_{\boldsymbol{k}}^{(n)} + \Delta t/\xi[\eta(z)M(A)|\nabla\phi^{(n)}| - \gamma\frac{G'(\phi^{(n)})}{\epsilon^2} + (\boldsymbol{F}_{sub}+\boldsymbol{F}_{geo})\cdot\nabla\phi^{(n)}]_{\boldsymbol{k}}}{1+\Delta t\gamma k^2/\xi}.$$

Eq.S6&S7 are discretized using the forward Euler scheme with $\partial_t(\psi A) = \psi^{(n)}(A^{(n+1)}-A^{(n)})/\Delta t + A^{(n)}(\psi^{(n+1)}-\psi^{(n)})/\Delta t$. The diffusion terms $\nabla\cdot(\psi\nabla A)$ are also approximated using finite difference. The x-term, for example, reads $[(\psi_{i+1,j}+\psi_{i,j})(A_{i+1,j}-A_{i,j})/(2\Delta x) - (\psi_{i,j}+\psi_{i-1,j})(A_{i,j}-A_{i-1,j})/(2\Delta x)]/\Delta x$. The white noise terms are simulated as Wiener processes with $\zeta(t)\Delta t = \sqrt{\sigma\Delta t}N(0,1)$. Mass conservation is enforced for the activator but not for the inhibitor. We avoid any negative values by introducing setting the value of the inhibitor to zero whenever it becomes negative. In practice, however, this does not occur due to the small value of the added noise.

As initial condition for ϕ, we use a cylinder with surface size S_0 and volume V_0. The activator and inhibitor concentration outside the boundary is 0. To implement this boundary condition, we solve Eq.S6&S7 only for $\phi > 5\times10^{-5}$, and set $A = R = 0$ outside this region.

REGULATION FROM SUBSTRATE ON BIOCHEMICAL MODULE

As mentioned in the main text, the model can also produce different migration modes when a biochemical, rather than a mechanical parameter, becomes z dependent. For example, we can make the activation rate of the inhibitor c_2 vary as a function of z:

$$c_2(z) = c_b + (c_t - c_b)[1+\tanh(z-h)]/2, \tag{S9}$$

In this case, close to the substrate we have $c_2 = c_b$ while far away from the substrate $c_2 = c_t$. In between, c_2 changes gradually and this change is maximal at $z = h$.

In our simulations, we have taken $c_t = 8$ so that the top part of the cell is not excitable nor oscillatory. As a result, wave propagation is constrained to the basal surface bottom. The simulation results of varying c_b and protrusive

strength parameter η_0 are shown in Fig. S4. By changing c_b, we can reproduce the amoeboid-like, oscillatory and fan-shaped cell morphologies, similar to Fig. 5 in the main text. Furthermore, the oscillatory cells show a periodic area and height dependence. For this model variant, however, activator patches in the amoeboid-like cells only occur at the cell-substrate interface. Notably, by changing the protrusive force, we can observe transitions of fan-shaped cells to cells with unstable waves, similar to our earlier studies [10]. Those cells move like amoeboid cells with random polarity while the basal surface area changes are irregular compared to the oscillatory cells (Fig. S4).

REFERENCES

[1] Shao, D., Rappel, W.-J. & Levine, H. Computational model for cell morphodynamics. *Physical Review Letters* **105**, 108104 (2010).

[2] Shao, D., Levine, H. & Rappel, W.-J. Coupling actin flow, adhesion, and morphology in a computational cell motility model. *Proc Natl Acad Sci U S A* **109**, 6851–6856 (2012).

[3] Camley, B. A. *et al.* Polarity mechanisms such as contact inhibition of locomotion regulate persistent rotational motion of mammalian cells on micropatterns. *Proc Natl Acad Sci U S A* **111**, 14770–14775 (2014).

[4] Alamo, J. C. D. *et al.* Spatio-temporal analysis of eukaryotic cell motility by improved force cytometry. *PNAS* **104**, 13343–13348 (2007).

[5] Lombardi, M. L., Knecht, D. A., Dembo, M. & Lee, J. Traction force microscopy in dictyostelium reveals distinct roles for myosin II motor and actin-crosslinking activity in polarized cell movement. *J Cell Sci* **120**, 1624–1634 (2007).

[6] Zimmermann, J., Camley, B. A., Rappel, W.-J. & Levine, H. Contact inhibition of locomotion determines cell–cell and cell–substrate forces in tissues. *Proceedings of the National Academy of Sciences* **113**, 2660–2665 (2016).

[7] Cao, Y. *et al.* Cell motility dependence on adhesive wetting. *Soft Matter* **15**, 2043–2050 (2019).

[8] Arai, Y. *et al.* Self-organization of the phosphatidylinositol lipids signaling system for random cell migration. *Proc. Natl. Acad. Sci. U.S.A.* **107**, 12399–12404 (2010).

[9] Gerhardt, M. *et al.* Actin and pip3 waves in giant cells reveal the inherent length scale of an excited state. *J Cell Sci* **127**, 4507–4517 (2014).

[10] Cao, Y., Ghabache, E. & Rappel, W.-J. Plasticity of cell migration resulting from mechanochemical coupling. *bioRxiv* 644880 (2019).

FIGURES

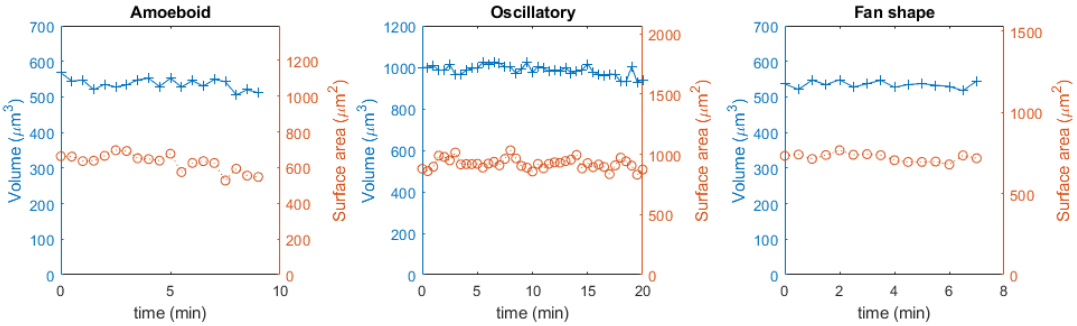

FIG. S1: The total volume (blue symbols) and the total surface area (orange symbols) for each migration mode for the cells in Fig. 2 of the main text.

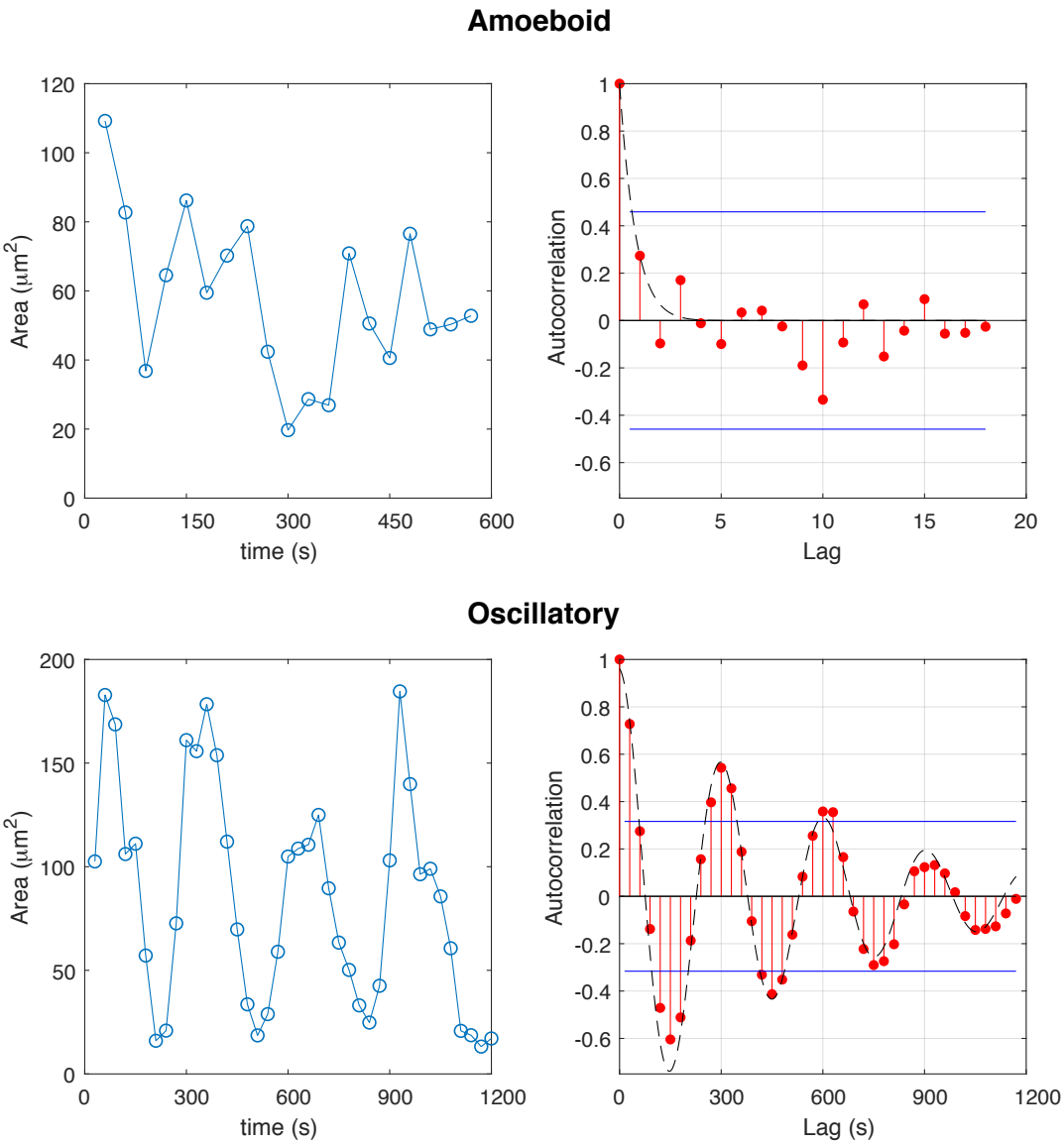

FIG. S2: Basal surface area as a function of time (left panels) and corresponding autocorrelation (right panels) for the amoeboid and oscillating cell shown in Fig. 2 of the main text. The blue horinzontal lines in the autocorrelation plots represent the 95%-confidence interval and the dashed line shows a fit to an exponentially decaying sinusoidal function $cos(2\pi t/T)exp^{-t/\tau_{decay}}$. For the amoeboid cell, the period T and decay time τ_{decay} were found to be 24 s and 600 s, respectively. For the oscillating cell, these values are 570 s and 300 s.

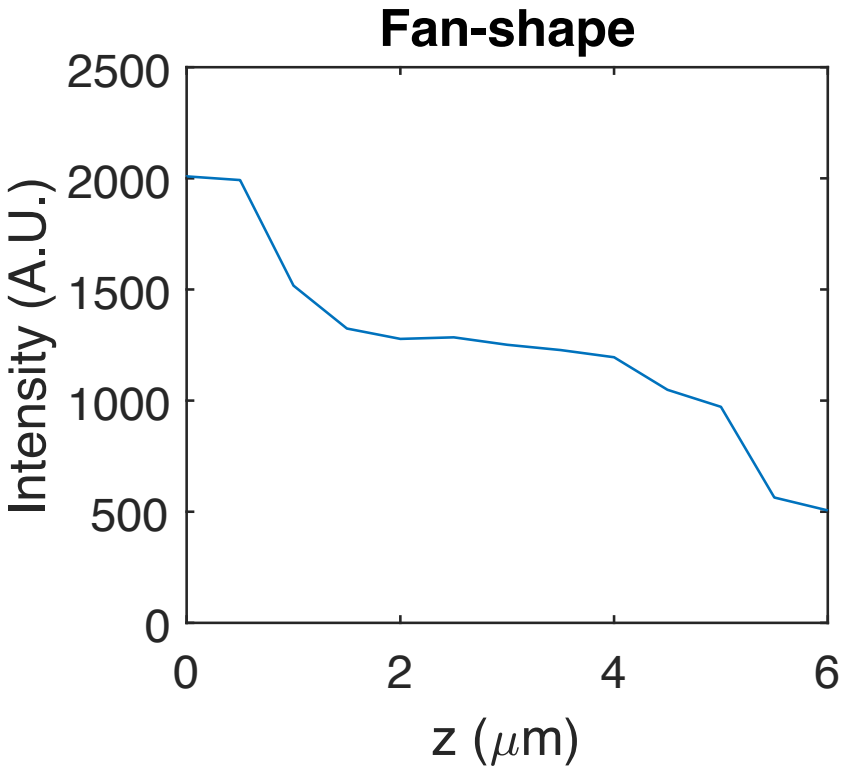

FIG. S3: Total time-averaged limE-GFP fluorescence as a function of height for a fan-shaped cell.

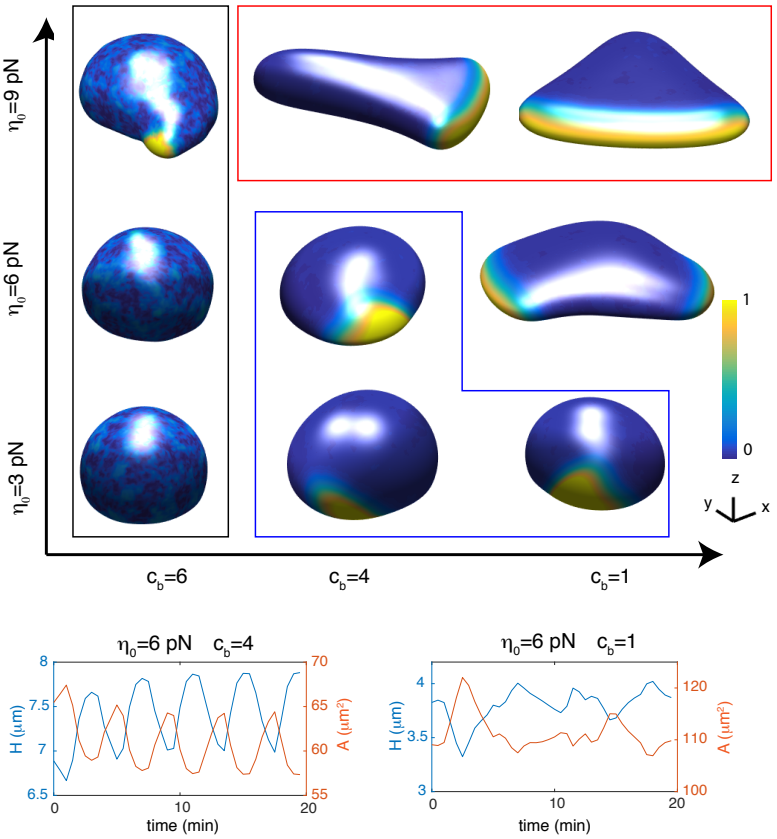

FIG. S4: Snapshots of cell morphologies (front view) in the c_b, η_0 phase space, with $c_2(z)$ given by Eq. S8. The activated membrane-bound activator is plotted using the color scheme indicated by the bar. Cells within the black frame are amoeboid, within the blue frame are oscillatory, and within the red frame are fan-shaped. The cell with $\eta_0 = 6, c_b = 1$ shows random migration with unstable waves at the bottom, and the basal surface area size changes irregularly, compared to the oscillatory cells with $\eta_0 = 6, c_b = 4$.

Parameter	Description	Value
γ	Tension parameter	3 pN μm
ϵ	Width of phase field	1.5 μm
B_V	Cell volume conservation strength	10 pN/μm^3
B_S	Cell surface conservation strength	10 pN/μm^2
V_0	Cell volume	$350\mu m^3$
S_0	Cell surface	$300\mu m^2$
h	height of the half-maximum protrusive force	3μm
h_0	length scale of the protrusive force variation	2μm
f_{adh}	Cell-substrate adhesion strength	1 pNμm
f_{rep}	Cell-substrate repellent strength	20 pN
ξ	Friction coefficient	1.25 pN min/μm^2
k_a	Activation rate	40 min^{-1}
K_a	Activation threshold	1 μM
b	Basal activation rate	0.4 μM min^{-1}
A_t	Total activator concentration($= N_{tot}/V_0$)	2 μM
α	Activator activation coefficient	5
d_1	Basal degradation rate	4 min^{-1}
d_2	Degradation rate from inhibitor	4 $\mu\text{M}^{-1}\text{min}^{-1}$
c_1	Inhibitor degradation coefficient	1
τ	Time scale of negative feedback	1.25 min
D_A	Activator diffusion coefficient	2 μm^2/min
D_R	Inhibitor diffusion coefficient	2 μm^2/min
σ	Noise intensity	0.04 $\mu\text{M}^2/\mu\text{m}^3$/min
Δt	Time step	0.001 min
l, n, m	Space grid size	128, 128, 128
$L_{x,y,z}$	Space size	20,20,20 μm

TABLE S1: Model Parameters

MOVIES

Movie S1: Migration of a keratocyte-like with the actin distribution visualized with the fluorescent marker limE-GFP.

Movie S2: Side view of an oscillatory cell expressing the fluorescent marker limE-GFP, obtained using LLSM.

Movie S3: LimE-GFP dynamics of an oscillatory cell, visualized using LLSM, in the basal plane (top), and in a cross-sectional plane perpendicular to the substrate (bottom).

Movie S4: Simulated amoeboid-like cell with the membrane-bound activator distribution displayed using the color scheme and parameters of Fig. 4.

Movie S5: Oscillatory cell obtained in simulations with the membrane-bound activator distribution displayed using the color scheme and parameters of Fig. 4.

Movie S6: Simulated keratocyte-like cell with the membrane-bound activator distribution displayed using the color scheme and parameters of Fig. 4.